MedChemComm

Cite this: *Med. Chem. Commun.*, 2012, **3**, 592

www.rsc.org/medchemcomm

CONCISE ARTICLE

Biological and computational evaluation of an oxadiazole derivative (MD77) as a new lead for direct STAT3 inhibitors†

Daniela Masciocchi,[a] Stefania Villa,[a] Fiorella Meneghetti,[a] Alessandro Pedretti,[a] Daniela Barlocco,[a] Laura Legnani,*[b] Lucio Toma,[b] Byoung-Mog Kwon,[c] Shintaro Nakano,[d] Akira Asai[d] and Arianna Gelain*[a]

Received 25th January 2012, Accepted 27th February 2012
DOI: 10.1039/c2md20018j

Signal Transducer and Activator of Transcription 3 (STAT3) is a latent cytoplasmic protein overexpressed in various cancer cell lines. STAT3 participates in oncogenesis by stimulating cell proliferation and preventing apoptosis and it has been proven as a suitable target for anticancer therapy. In order to identify direct STAT3 inhibitors, we performed a binding assay on several previously synthesized 1,2,5-oxadiazole derivatives. Among them, compound **MD77**, *N*-[4-(4-chlorophenyl)-1,2,5-oxadiazol-3-yl]-4-(trifluoromethyl)benzamide, showed a good ability to bind the STAT3–SH2 domain in a dose-dependent manner (IC_{50} = 17.7 μM). Computational studies were carried out to investigate its binding mode. Moreover, compound **MD77** showed a significant anti-proliferative activity *versus* several tumor cell lines. On these bases, compound **MD77** was selected as a lead for the future development of direct STAT3 inhibitors.

Introduction

Signal Transducers and Activators of Transcription (STATs) are a family of cytoplasmic proteins which have two critical roles: to transduce signals through the cytoplasm and to act as transcription factors in the nucleus. Seven STAT family members, encoded by distinct genes, were identified, namely STAT1 to STAT4, STAT5a, STAT5b and STAT6.[1] They are constituted by several structurally and functionally conserved domains: the *N*-terminal coiled-coil (involved in STAT dimer–dimer interactions), the DNA binding domain (responsible for complex formation between STAT proteins and DNA), the Src homology 2 (SH2) (a linker region required for the recruitment of STAT monomers through reciprocal *p*Tyr–SH2 domain interaction), and finally the *C*-terminal transactivation domain (as transcriptional activation domain).[2] The STATs activation cascade involves the phosphorylation of a specific tyrosine residue, which allows the protein dimerization and translocation to the nucleus where STATs are able to modulate gene transcription through a direct binding to DNA.

In particular, STAT3 is constitutively activated in a wide variety of human solid and blood tumors[3,4] as a result of a deregulation of cytokine receptors, growth factors and Janus kinases (JAK) activity.[5,6] The inhibition of STAT3 signaling leads to growth arrest and apoptosis of various cancer cell lines, suppresses cancer cell survival, and induces tumor regression,[7–9] having no effects in normal cells.[10] For these reasons, STAT3 can be considered a promising target for anticancer therapy. STAT3 signaling can be inhibited through direct interaction of molecules with the protein or by indirect inhibition of the upstream tyrosine kinases or blockage of other factors involved in the activation.[11] Since the indirect approach is endowed with a poorly specific mechanism of action that could cause important adverse effects,

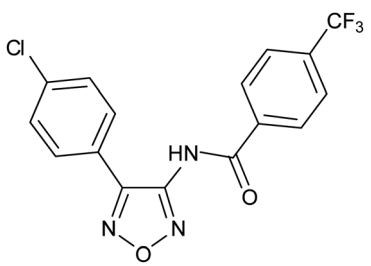

MD77

[a]*Dipartimento di Scienze Farmaceutiche "P. Pratesi", Università degli Studi di Milano, Via L. Mangiagalli 25, 20133 Milano, Italy. E-mail: arianna.gelain@unimi.it; Fax: +39-02-503-19359; Tel: +39-02-503-19369*
[b]*Dipartimento di Chimica, Università degli Studi di Pavia, Via Taramelli 12, 27100 Pavia, Italy. E-mail: laura.legnani@unipv.it; Fax: +39-0382-98-7323; Tel: +39-0382-98-7311*
[c]*Laboratory of Chemical Biology and Genomics, Korea Research Institute of Bioscience & Biotechnology and Department of Biomolecular Science, Korea University of Science and Technology, Eoun-Dong, Yuseong-gu, Daejeon 305-333, South Korea*
[d]*Center for Drug Discovery, Graduate School of Pharmaceutical Sciences, University of Shizuoka, 52-1 Yada, Suruga-ku, Shizuoka, 422-8526, Japan*

† Electronic supplementary information (ESI) available: Synthetic procedures and NMR spectra of **MD77**, chemical structure of compound **1**, conformational studies of compound **1**, docking pose of conformer **C** of **MD77**, mean graphs and dose–response parameters. CCDC reference number 853297. For ESI and crystallographic data in CIF or other electronic format see DOI: 10.1039/c2md20018j

the challenge is the discovery of new selective and direct STAT3 inhibitors.

In a previous paper,[12] we studied, as potential STAT3 inhibitors, three series of 1,2,5-oxadiazoles, bearing at position 3 a ureido, carboxamido, and sulfonamido function, respectively. All the synthesized compounds were evaluated in a dual-luciferase assay at a concentration of 2 μM, in order to determine their ability to lower STAT3 activity. The interesting results led us to investigate if these compounds were able to directly interact with STAT3. Therefore, they were submitted to the AlphaScreen-based assay,[13] an *in vitro* competitive binding test used to identify compounds able to directly inhibit the binding of SH2-containing proteins to their correspondent phosphopeptides, the physiological ligands. Quite unexpectedly, only *N*-[4-(4-chlorophenyl)-1,2,5-oxadiazol-3-yl]-4-(trifluoromethyl)benzamide (**MD77**) proved to be able to significantly interact with the SH2 domain.

In parallel, **MD77** was retested in the dual-luciferase assay[14] at a higher concentration (5 μM) and its anti-proliferative activity was evaluated on a panel of 58 cancer cell lines. Here we report the biological results, the solid state characterization, and the modeling and docking studies of **MD77**, as a new direct inhibitor of STAT3.

Results and discussion

Biological studies

AlphaScreen-based assay. To investigate the direct binding properties of several 3,4-disubstituted-1,2,5-oxadiazoles[12] to the SH2 domain we performed the AlphaScreen-based assay,[13] as described in the Experimental section. In particular, besides STAT3, other SH2-containing proteins, such as STAT1 and Grb2 ("Growth factor receptor-bound protein 2"), having a high degree of sequence homology to STAT3 (78% and 65%, respectively) were tested. **MD77** was the only compound with a significant activity *versus* STAT3 (72.0% of inhibition at a concentration of 30 μM). Moreover, it selectively antagonized the STAT3–SH2 domain with respect to the Grb2–SH2 domain (72.0% *versus* 10.5% at 30 μM concentration), although it exhibited a higher affinity toward the STAT1–SH2 domain (94.6% *versus* 72.0% at 30 μM concentration).

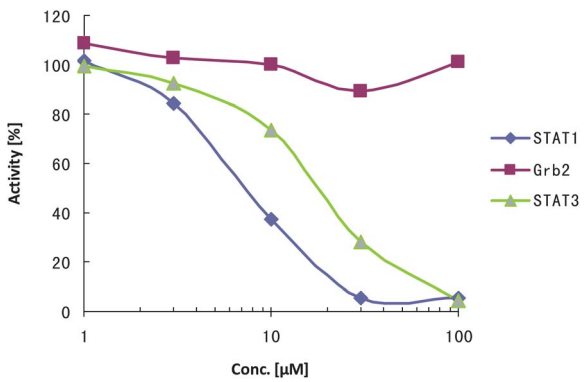

Fig. 1 Dose–response curves of the inhibition of STAT3, STAT1, and Grb2 binding to *p*Tyr-containing peptides by compound **MD77** as determined by AlphaScreen-based assay (% of activity *versus* concentration expressed in logarithmic scale).

Its inhibitory activity proved to be dose-dependent (Fig. 1) with calculated IC_{50} values of 17.7 μM for STAT3, 7.2 μM for STAT1 and higher than 100 μM for Grb2.

Dual-luciferase assay. The STAT3 inhibitory activity of **MD77** was evaluated in a dual-luciferase assay,[14] at a higher concentration (5 μM) with respect to the published data (2 μM),[12] in human colorectal carcinoma cells HCT-116, characterized by uncontrolled expression of STAT3 (see Experimental section). The results showed that **MD77** exhibits an interesting percentage of inhibition (20%).

Chemistry

MD77 was synthesized following slightly modified literature methods.[12] The synthetic procedure consists of six steps with most of the yields higher than 90% and only two purifications by flash chromatography (see ESI†).

X-Ray and conformational analysis of MD77

The crystallographic structure of **MD77** is represented in Fig. 2.

Bond lengths and angles assume the expected standard values. The overall conformation of the compound is defined by four torsional angles: N2–C2–N3–C11 (τ_1) of −118(1)°, C2–N3–C11–C5 (τ_2) of 175(1)°, N3–C11–C5–C6 (τ_3) of −150(1)° and C2–C1–C3–C13 (τ_4) of 22(1)°. The oxadiazole ring is rotated by 25(1)° and 88(1)° with respect to the chlorophenyl- and trifluoromethylphenyl moieties, respectively. The latter two rings are perpendicularly oriented with respect to each other, with a dihedral angle of 87(1)°. The analysis of the crystal packing has evidenced the important role played by the halogen atoms in connecting adjacent molecules, through Cπ–H···F, Cπ–H···Cl and C=O···F type contacts, influencing in this way the molecular conformation. Besides, the oxadiazole ring gives rise, in the crystal, to π interactions with the chloro-phenyl group of symmetry related molecules along the *b* axis, indicating the ability of the compound to interact through molecular stacking with a biological counterpart.

The crystallographic structure represents only one of the accessible molecular conformations. Thus, a complete modeling study of **MD77** was carried out, considering all the degrees of

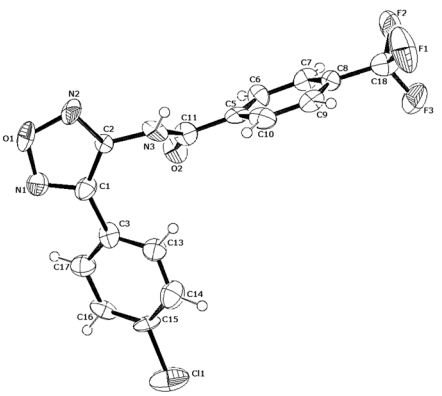

Fig. 2 ORTEP[15] view of **MD77** and the relative arbitrary atom-numbering scheme (thermal ellipsoids at 40% probability).

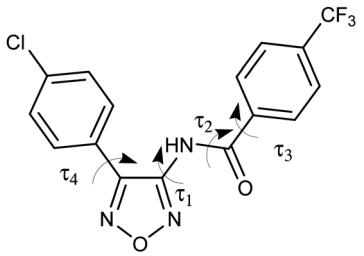

Chart 1 **MD77** conformational degrees of freedom.

Table 1 Relative energies, equilibrium percentages, and significant torsional angles of the minimum energy conformations of **MD77**

	E_{rel} vacuo (kcal mol^{-1})	P vacuo (%)	E_{rel} water/ kcal mol^{-1}	P water (%)	τ_1 (°)	τ_2 (°)	τ_3 (°)	τ_4 (°)
A	2.10	1.9	0.00	40.9	22	−177	−154	43
B	2.49	1.0	0.17	30.6	0	177	−158	−48
C	0.00	65.0	0.28	25.5	−126	174	−159	34
D	0.42	32.1	1.53	3.0	−110	174	−156	−45

conformational freedom that correspond to the above defined torsional angles (Chart 1) and, in particular, the arrangement of the amidic group with respect to the oxadiazole ring. The geometry optimizations were performed at the B3LYP/6-311+G(d,p) level[16] and the energy of the optimized conformations was recalculated using a polarizable continuum solvent model (PCM)[17] to take into account the effect of water.

Four minimum energy conformations were located and in Table 1 their geometrical descriptors (τ_1–τ_4) are reported, together with their gas-phase and water-solvated energies and the corresponding percentage contributions to the overall population. It is worth pointing out that a mirror image conformation exists for each described conformation; thus, the number of conformations accessible to the molecule is double with respect to those reported.

Conformations **A** and **B** are very similar (Fig. 3), as evidenced by their values of τ_1, τ_2, and τ_3, the only difference being the orientation of the *p*-chlorophenyl ring (τ_4). The same occurs for the couple **C** and **D**. The most stable conformation in water (**A**) accounts for 40.9% of the overall population and, together with conformation **B**, represents 71.5%, the remaining not negligible 28.5% being due to the *in vacuo* preferred conformations **C** and **D**.

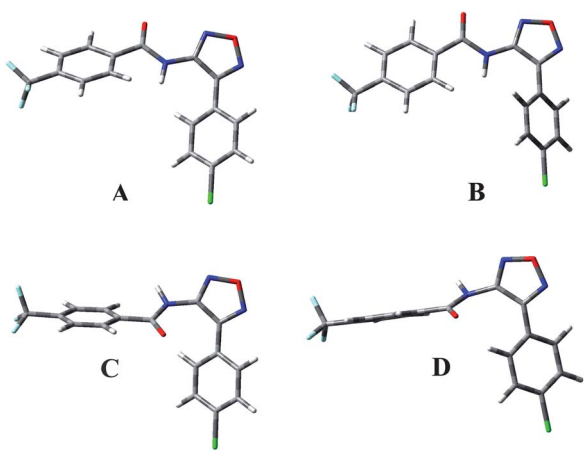

Fig. 3 3D plots of conformations **A–D** of compound **MD77**.

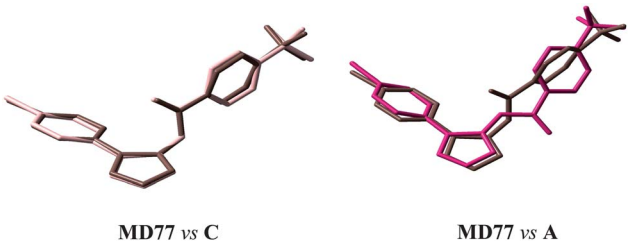

Fig. 4 Superimposition of the crystal structure of compound **MD77** (brown) onto the **C** (pink) and **A** (magenta) conformers obtained through rms fitting of the heavy atoms. Hydrogen atoms are omitted for the sake of clarity.

A comparison of conformations **A–D** with the above described crystal structure of **MD77** shows that it corresponds to **C**, which is the most stable conformation *in vacuo*. In fact, the two structures are characterized by about the same values of τ_1–τ_4 and the overlay of their heavy atoms produces an almost perfect superimposition (Fig. 4) with a rms difference value of 0.191 Å. By contrast, the comparison of the solid state structure with conformer **A** gives a rms difference value of 1.067 Å. The crystal structure and conformer **A** orient their amide function in very different directions (Fig. 4), as evidenced by the significantly different values of τ_1: −118(1)° in the crystal *versus* 22° in **A**. The amide function usually represents a key moiety for anchoring a ligand at the binding site of the protein and the ability of **MD77** to vary the orientation of the amide under different conditions is worthy of note. The orientation in the crystal is determined by packing interactions, as the molecules form chains through the hydrogen bond N3–H3···O2^{i} (^{i} at x, $y-1$, z), forcing in some way the molecular bending and favoring the conformation having the carbonyl oxygen pointing in the opposite side with respect to the chlorophenyl group.

Docking studies

Docking studies were performed on **MD77** in order to investigate its interaction with the SH2 domain. In particular, considering the STAT3–**MD77** complex and the conformational profile

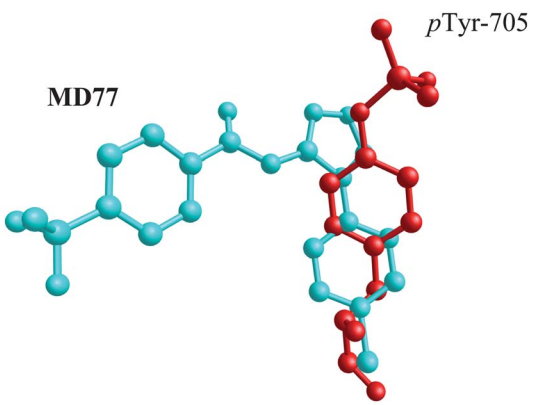

Fig. 5 Comparison of **MD77** (cyan) in the docking pose with the *p*Tyr-705 (red) of the second subunit in the STAT3 dimer.

of the ligand, the best scored pose showed that the ligand assumes the most stable conformation **A**. The binding mode of **MD77** is comparable to that of phosphorylated Tyr-705, because it involves the same pocket in which *p*Tyr-705 is inserted when two subunits are assembled in the dimer. The phenyloxadiazole moiety of **MD77**, colored in cyan, occupies the same pocket (not shown) of *p*Tyr-705, colored in red (Fig. 5).

This pocket is placed on the protein surface and is surrounded by hydrophilic and polar amino acids to better interact with the negatively charged side chain of the phosphorylated tyrosine, mimed by the phenyloxadiazole moiety in the STAT3–**MD77** complex.

As shown in Fig. 6, the favored conformation **A** of **MD77** establishes many hydrogen bond interactions within the binding pocket. In detail, they involve the trifluoromethyl group of the aromatic ring and the guanidine moiety of Arg-595 by three hydrogen bonds, the oxygen of the amidic group and the amine of side chain of Lys-591 by one hydrogen bond, the oxygen and the nitrogen atoms of the oxadiazole ring and the guanidine group of Arg-609 by two hydrogen bonds and finally the chlorine atom of the aromatic ring with one amidic hydrogen of the Gln-635 side chain.

Despite the presence of three aromatic rings in **MD77**, π–π interactions were not found in its complex with the macromolecule, due to the absence of aromatic amino acids in the binding pocket. Analyzing the other **MD77** complexes obtained by docking, it was possible to identify a pose in which the ligand assumes a conformation referable to the couple **C–D**, but its interaction energy is worse than all calculated complexes and the binding mode is much different if compared to the most stable conformation shown above. In particular, the *p*-trifluoromethylphenyl group is partially inserted in the *p*Tyr-705 pocket while, in the best complex, this pocket is occupied by the oxadiazole ring. In this complex, the oxadiazole ring does not mime the phosphate and stabilizes the complex through

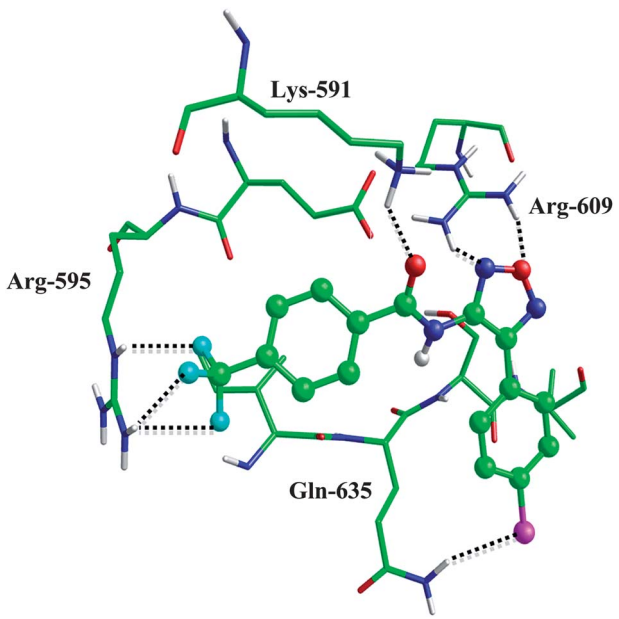

Fig. 6 Main interactions between **MD77** and STAT3. The hydrogen bonds are shown as dotted lines.

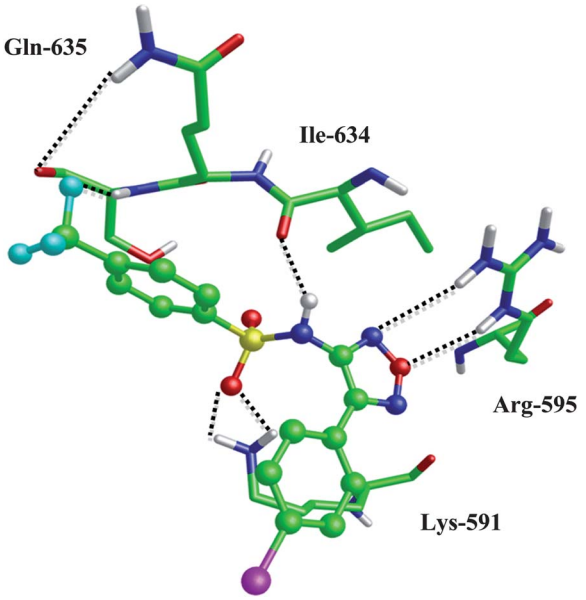

Fig. 7 Main interactions between compound **1** and STAT3. The hydrogen bonds are shown as dotted lines.

hydrogen bonds with Gln-635 and Lys-626 (see ESI†). Finally, one of the poses of **MD77** corresponds to the mirror image of conformation **A**. It presents a different binding mode in which the *p*Tyr-705 pocket is not occupied, losing the interaction with Arg-609, but keeping the weak hydrogen bonds between Arg-595 and the trifluoromethyl group.

It should be noted that the sulfonamido bioisoster (**1**) of **MD77**, which was found inactive both in the AlphaScreen and in the dual-luciferase assays, has a different conformational behavior with respect to our lead compound. In fact, none of the localized conformations of **1** shows a relative arrangement of the aromatic groups similar to that displayed in the four geometries of **MD77** (see ESI†). Thus, the identification of its binding mode through docking calculations seemed to be important to clarify the essential features for an efficient interaction with STAT3 (Fig. 7).

Considering the STAT3-compound **1** complex, the pose and interacting conformation of the ligand are much different from those shown by **MD77**. In particular, compound **1** is unable to occupy the *p*Tyr-705 pocket and the oxadiazole ring interacts with Arg-595 instead of Arg-609, which is the key residue involved in the **MD77** complex and in the formation of the salt bridge with the phosphate group when the protein dimerizes. Despite the different binding mode, the compound **1** complex is stabilized by an extended network of hydrogen bonds, shown in Fig. 7. In the docked conformation of compound **1** the two benzene rings are perpendicular, the angle between them (89°) being significantly higher than the corresponding value (28°) found for **MD77** in the best score pose.

Anti-proliferative assay

In order to verify the anti-proliferative activity of compound **MD77**, cell proliferation assays were performed by NCI (Bethesda, USA) under the Developmental Therapeutic Program (DTP) to determine its effect on tumor cells growth. **MD77** was

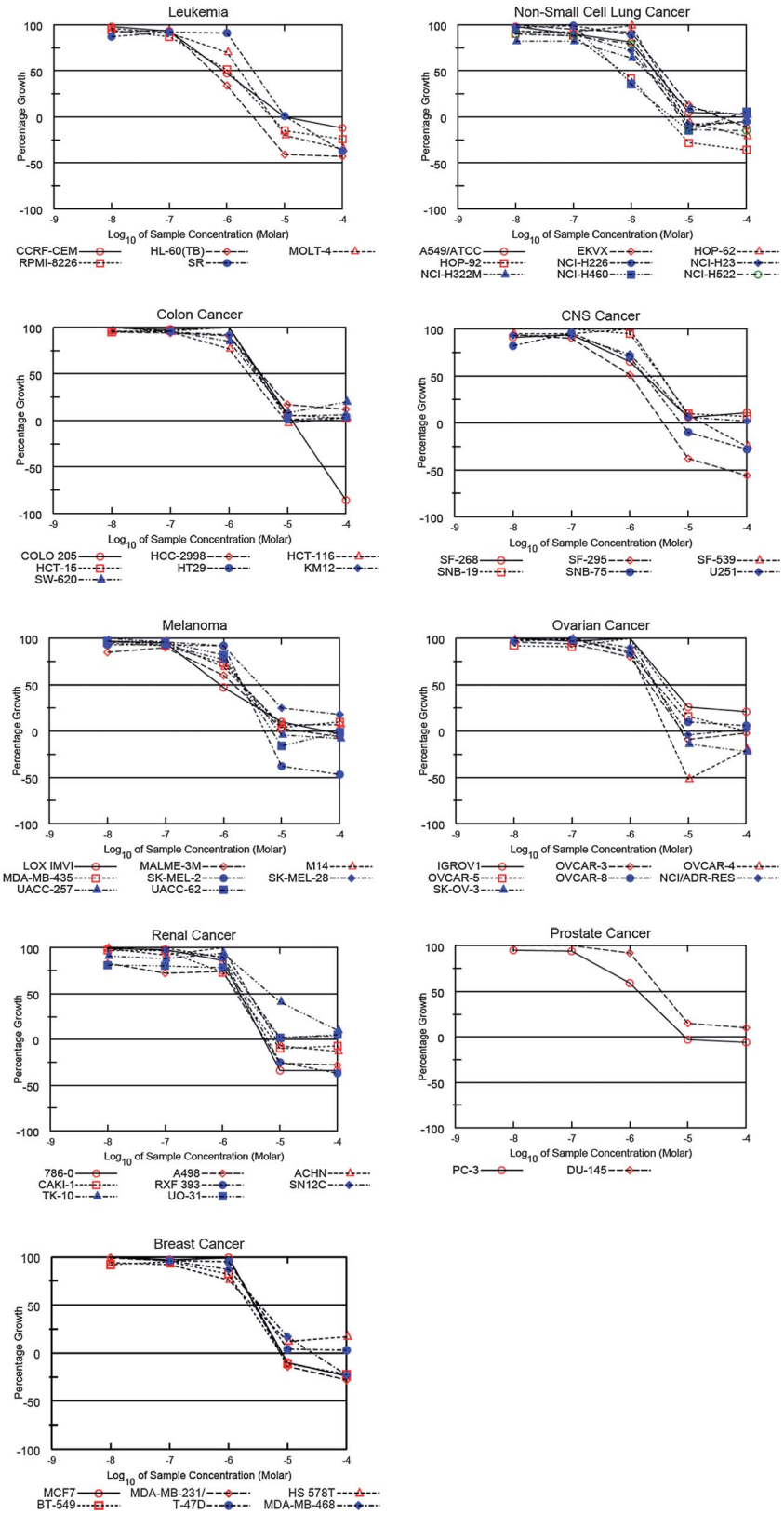

Fig. 8 Dose–response curves showing the percentage growth inhibition of compound **MD77** in panel/cell lines (data obtained from NCI *in vitro* disease oriented tumor cell screen).

exposed to a panel of 58 human tumor cell lines, derived from 9 cancer cell types, and it was firstly tested at a single dose of 10 μM[18] (see Experimental section).

Since it exhibited a significant growth inhibition value, it was subjected to a complete analysis at five different doses for 48 hours. The data are expressed as dose–response parameters GI_{50}, TGI and LD_{50} referred to **MD77** molar concentration that produces 50% of growth inhibition, total growth inhibition and 50% of cytotoxicity, respectively (see ESI†). In these assays **MD77** exhibited a good profile of inhibitory activity on cell proliferation, with GI_{50} values ranging from 6.75×10^{-6} M (renal cancer, TK10) to 5.46×10^{-7} M (leukemia, HL60TB), and showing TGI values lower than 1.00×10^{-4} M in most of the cell lines (the dose–response parameters expressed as mean graph are reported in the ESI†).

The dose–response curves showing the activity of **MD77** on the panel/cell lines are represented in Fig. 8. As expected, **MD77** inhibits the growth of the cell lines which are known to over-express STAT3 (for instance HCT116, DU145, and MDA-MB-231), although several cell lines, such as HL60TB (leukemia cells) and HOP-92 (non-small cells lung cancer), are the most sensitive.

Conclusions and future perspectives

The ability to target the STAT3–SH2 domain of a series of oxadiazole derivatives was evaluated in order to identify new, direct inhibitors. One compound (**MD77**) proved to be able to significantly interact with the SH2 domain: in the AlphaScreen binding assay, it showed an interesting dose–response profile with an IC_{50} value of 17.7 μM. This result highlighted its potential as a protein–protein interaction inhibitor. In addition, **MD77** exhibited a significant activity (20% inhibition at 5 μM) in a dual-luciferase assay. To investigate the conformational behavior and the binding mode of **MD77**, modeling and docking studies were performed. The latter evidenced that in the best scored pose of the **STAT3–MD77** complex, **MD77** assumes the most stable conformation calculated in water. It should be noted that the binding mode of **MD77** is comparable to that of *p*Tyr-705, when the latter is involved in the formation of the STAT3 dimer. The computational data were supported by crystallographic studies. Finally, **MD77** displayed a significant growth inhibitory activity on a number of tumor cell lines. In the light of these interesting results, **MD77** emerged as a lead for the development of a new series of derivatives that is actually underway.

Experimental

AlphaScreen-based assay

AlphaScreen is a bead-based nonradioactive assay system for detecting biomolecular interactions in a microtiter plate format. Binding of biological partners brings donor and acceptor beads into close proximity and as a result, a fluorescent signal between 520 and 620 nm is produced. The AlphaScreen-based assays[13] were performed in a final reaction volume of 25 μL of the assay buffer containing 10 mM HEPES–NaOH (pH 7.4), 50 mM NaCl, 1 mM EDTA (pH 8.0), 0.1% NP-40, and 10 ng μL^{-1} BSA in a 96-well microtiter plate at 25 °C. Phospho-Tyr (*p*Tyr) peptide probes used in this study were 5-carboxyfluorescein (FITC)-GpYLPQTV for STAT3, FITC-GpYDKPHVL for STAT1, and FITC-PSpYVNVQN for Grb2. Firstly, 75 nM of each SH2-containing protein was incubated with the test compound for 15 min. Each protein sample was then incubated for 90 min with 50 nM of its corresponding FITC-*p*Tyr peptide, and mixed with streptavidin coated donor beads and anti-FITC acceptor beads simultaneously before detection at 570 nm using EnVison Xcite (PerkinElmer).

Dual-luciferase assay

Cell culture. The cancer cell lines were obtained from American Type Culture Collection. Human breast cancer cell lines (MDA-MB-468 and MDA-MB-231) and the human colon cancer cell line (SW620) were maintained in RPMI 1640 (Gibco/BRL). Another human colon cancer cell line (HCT-116) was maintained in McCoy's 5A (Gibco/BRL). All culture media were supplemented with 10% heat-inactivated fetal bovine serum (Gibco/BRL). Cell cultures were maintained at 37 °C under a humidified atmosphere of 5% CO_2 in an incubator.

Transient transfection and dual-luciferase assays.[14] HCT-116 cells were seeded at a density of 10×10^5 cells in 100 mm^2 culture plate. The cells were co-transfected with pSTAT3-TA-Luc (27 μg per plate) and an internal control plasmid pRL-TK (9 μg per plate) containing the *Renilla* luciferase gene. All plasmids used in this experiment were purchased from Promega. The transfection was carried out using TransFectin (Bio-Rad), according to the manufacturer's protocol. After 5 h of transfection, the cells were trypsinized and seeded onto sterilized black bottom 96-well plates at a density of 1×10^4 cells per well. On the following day, cells were treated with test compounds and incubated for 24 h. Firefly and *Renilla* luciferase activities were measured using a dual-light reporter gene assay kit (Promega) on Wallac Victor2 (Perkin-Elmer, Inc., Wellesley, MA). *Renilla* luciferase activity was determined to calibrate transfection efficiency and cytotoxicity of chemicals. Relative STAT3 activity was calculated by dividing the firefly luciferase activity with *Renilla* luciferase activity in each transfection experiment. The values of STAT3 inhibitory activity were the means of 3 experiments and the maximum deviation from the mean was less than 10%.

Cell proliferation assay. Cells were seeded at a density of 5000 cells per well in 96-well plates in RPMI 1640 or McCoy's medium containing 10% FBS. They were replenished with fresh complete medium containing either test compound or 0.1% DMSO. After incubation for 24 or 48 h, the cell proliferation reagent WST-1 (Roche Applied Science) was added to each well. WST-1 formazan was quantitatively measured at 450 nm using an enzyme-linked immunosorbent assay reader (Bio-Rad).

Crystallography

Crystals of **MD77** were obtained from an ethanol solution at room temperature as white platelets. The intensity data were collected on an Enraf Nonius CAD-4 diffractometer with Mo Kα radiation ($\lambda = 0.71073$ Å) at room temperature. The lattice parameters were determined by least-squares refinements of 25 high angle reflections. Crystal system: monoclinic (*Pc*), cell dimensions (Å): $a = 11.115(3)$, $b = 5.008(3)$, $c = 14.112(5)$, $\beta =$

92.28(1). Final R indices [$I > 2s(I)$] $R1 = 0.044$, $wR_2 = 0.057$ for 1549 independent reflections. The structure was solved by direct methods[19] and the refinement was carried out with SHELX-97.[20] All non-H-atoms were refined anisotropically. The amidic H position was detected in a difference Fourier synthesis and refined with isotropic thermal factors, while the other hydrogen atoms were introduced at calculated positions in their described geometries and allowed to ride on the attached carbon atom with fixed isotropic thermal parameters (1.2 Ueq. of the parent carbon atom).†

Conformational analysis

The calculations were carried out using the Gaussian09 program package.[21] The conformational space of compound **MD77** was explored through optimizations at the B3LYP level with the 6-311+G(d,p) basis set.[16] Compound **1** was modeled at the same level as above (B3LYP/6-311+G(2df,p) level for the S atom). All the degrees of conformational freedom were considered paying particular attention to the possible arrangements of the amidic group with respect to the oxadiazole ring. The energy of the optimized conformations was recalculated in water using a polarizable continuum model (PCM).[17]

Molecular docking

The calculations were performed to evaluate the binding affinity of **MD77** and compound **1** with the STAT3–SH2 domain. STAT3 structure, co-crystallized with a DNA fragment, was downloaded from the Protein Data Bank[22] (PDB ID 1BG1[23]) and was dimerized applying the transformation matrix as reported in the PDB file. The model was completed adding the hydrogens in two steps: (1) to STAT3, applying the algorithm for proteins and (2) to DNA, applying the algorithm for nucleic acids. In both cases, we used the features included in the VEGA ZZ package.[24] Atom charges (the Gasteiger–Marsili method[25]) and potentials (CHARMM 22 for proteins[26] and nucleic acids[27]) were assigned to the obtained structure. Finally, the model was optimized through a conjugate gradients minimization (30 000 steps) in order to reduce the high-energy sterical interactions. In order to preserve the experimental data, atom constraints were applied to the protein and the DNA backbones. This step was carried out by NAMD 2.8[28] integrated in the VEGA ZZ graphic environment. Before running GriDock, the grid maps required to evaluate the docking score were calculated, selecting the atoms included in a sphere of 12 Å radius centered on phosphorylated Tyr-705 (PTR-705 in the PDB file), which is known to play a pivotal role in the STAT3 dimerization and activation. This phase was carried out by AutoGrid 4 interfaced to VEGA ZZ. **MD77** and compound **1** were docked by GriDock/AutoDock[29] using the genetic algorithm search and generating 20 possible solutions. All these complexes were minimized by NAMD (conjugate gradients, 10 000 steps), keeping the atoms fixed outside from the spheroid defined by a layer of 12 Å thickness around the ligand.

Cell proliferation assays

Compound **MD77** was sent to the *National Cancer Institute* (NCI) in Bethesda, Maryland (USA) and screened in a panel of 58 human tumor cell lines, derived from nine neoplastic cancer types (leukemia, lung, colon, CNS, melanoma, ovarian, renal, prostate, and breast cancers) to test its anti-proliferative activity. The screening was a two-stage process, beginning with the evaluation of the compounds against 58 human tumor cell lines at a single dose of 10 μM. These preliminary results are expressed as percentages of growth inhibition of treated cell lines per panel when compared to untreated control cells. **MD77** exhibited a significant growth inhibition and thus it was evaluated against the 58 cell panel at five concentration levels.

Methodology of the anti-proliferative assay. The anti-proliferative assay was performed according to the US NCI protocol.[18] Briefly, the human tumor cancer cell lines of the screening panel were grown in RPM 1640 medium containing 5% fetal bovine serum and 2 mM L-glutamine. Cells were inoculated into 96-well microtiter plates in 100 μL of complete medium at densities ranging from 5000 to 40 000 cells per well. The microtiter plates containing the cells were incubated for 24 h at 37 °C, 5% CO_2, 95% air and 100% relative humidity prior to addition of the experimental drug. **MD77** was solubilized in dimethyl sulfoxide at 400-fold the desired final maximum test concentration and stored frozen prior to use. At the time of drug addition, an aliquot of frozen concentrate was thawed and diluted twice to the desired final maximum test concentration with a complete medium containing 50 μg mL^{-1} gentamicin. Additional four-, 10-fold serial dilutions were made to provide a total of five drug concentrations plus control. Aliquots of 100 μL of these different drug dilutions were added to the appropriate microtiter wells already containing 100 μL of medium, resulting in the required final drug concentrations.

Following the addition of the compound, the plates were incubated for an additional 48 h at 37 °C, 5% CO_2, 95% air, and 100% relative humidity. Cells were fixed by the gentle addition of 50 μL of cold 50% (w/v) trichloroacetic acid (TCA) and incubated for 60 minutes at 4 °C. After washing with tap water and air drying, Sulforhodamine B (SRB) solution (100 μL) at 0.4% (w/v) in 1% acetic acid was added to each well, and plates were incubated for 10 minutes at room temperature. After removing the unbound dye by washing with 1% acetic acid, the bound stain was subsequently solubilized with 10 mM Trizma base and the absorbance was measured on a microplate reader.

Dose–response parameters (GI_{50}, TGI, LD_{50}) were calculated as reported in the NCI protocol.[18]

Acknowledgements

The authors thank Dr Kenji Matsuno for his fruitful support, CILEA (Milan) for the allocation of computer time, the Developmental Therapeutics Program, Division of Cancer Treatment and Diagnosis, National Cancer Institute[18] (Bethesda, USA) for conducting the cell proliferation assays and the Universities of Milan and Pavia for the financial support (PUR 2008 and FAR grants, respectively). B.-M. K. was supported by the National Research Foundation of Korea (NRF-2011-0015768).

Notes and references

1 J. E. Darnell, *Science*, 1997, **277**, 1630–1635.
2 J. Bromberg and J. E. Darnell, *Oncogene*, 2000, **19**, 2468–2473.

3 L. B. Mora, R. Buettner, J. Seigne, J. Diaz, N. Ahmad, R. Garcia, T. Bowman, R. Falcone, R. Faircloug, A. Cantor, C. Muro-Cacho, S. Livingstone, J. Karras, J. Pow-Sang and R. Jove, *Cancer Res.*, 2002, **62**, 6659–6666.
4 G. Niu, T. Bowman, M. Huang, S. Shivers, D. Reintgen, A. Daud, A. Chang, A. Kraker, R. Jove and H. Yu, *Oncogene*, 2002, **21**, 7001–7010.
5 L. Song, J. Turkson, J. G. Karras, R. Jove and E. B. Haura, *Oncogene*, 2003, **22**, 4150–4165.
6 U. M. Wegenka, J. Buschmann, C. Lutticken, P. C. Heinrich and F. Horn, *Mol. Cell. Biol.*, 1993, **13**, 276–288.
7 J. Turkson and K. Siddiquee, *Cell Res.*, 2008, **18**, 254–267.
8 S. O. Rahaman, P. C. Harbor, O. Chemova, G. H. Barnett, M. A. Vogelbaum and S. J. Haque, *Oncogene*, 2002, **21**, 8404–8413.
9 J. R. Grandis, S. D. Drenning, Q. Zeng, S. C. Watkins, M. F. Melhem, S. Endo, D. E. Johnson, L. Huang, Y. He and J. D. Kim, *Proc. Natl. Acad. Sci. U. S. A.*, 2000, **97**, 4227–4232.
10 W. M. Burke, X. Jin, H. J. Lin, M. Huang, R. Liu, R. Reynolds and J. Lin, *Oncogene*, 2001, **20**, 7925–7934.
11 D. Masciocchi, A. Gelain, S. Villa, F. Meneghetti and D. Barlocco, *Future Med. Chem.*, 2011, **3**, 367–397.
12 D. S. Shin, D. Masciocchi, A. Gelain, S. Villa, D. Barlocco, F. Meneghetti, A. Pedretti, Y.-M. Han, D. C. Han, M. Y. Han, B.-M. Kwon, L. Legnani and L. Toma, *Med. Chem. Commun.*, 2010, **1**, 156–164.
13 Y. Uehara, M. Mochizuki, K. Matsuno, T. Haino and A. Asai, *Biochem. Biophys. Res. Commun.*, 2009, **380**, 627–631.
14 B. A. Sherf, S. L. Navarro, R. R. Hannah and K. V. Wood, *Promega Notes*, 1996, **57**, 2–8.
15 C. K. Johnson, ORTEP 11, Report ORNL-5138, OakRidge National Laboratory, TN, 1976.
16 (*a*) C. Lee, W. Yang and R. G. Parr, *Phys. Rev. B: Condens. Matter Mater. Phys.*, 1988, **37**, 785–789; (*b*) A. D. Becke, *J. Chem. Phys.*, 1993, **98**, 5648–5652.
17 (*a*) E. Cancés, B. Mennucci and J. Tomasi, *J. Chem. Phys.*, 1997, **107**, 3032–3042; (*b*) M. Cossi, V. Barone, R. Cammi and J. Tomasi, *Chem. Phys. Lett.*, 1996, **255**, 327–335; (*c*) V. Barone, M. Cossi and J. Tomasi, *J. Comput. Chem.*, 1998, **19**, 404.
18 National Cancer Institute, http://dtp.nci.nih.gov.
19 A. Altomare, M. C. Burla, M. Camalli, G. Cascarano, C. Giacovazzo, A. Gagliardi and G. Polidori, *J. Appl. Crystallogr.*, 1994, **27**, 435.
20 G. M. Sheldrick, *SHELX-97*, University of Göttingen, Germany.
21 M. J. Frisch, G. W. Trucks, H. B. Schlegel, G. E. Scuseria, M. A. Robb, J. R. Cheeseman, G. Scalmani, V. Barone, B. Mennucci, G. A. Petersson, H. Nakatsuji, M. Caricato, X. Li, H. P. Hratchian, A. F. Izmaylov, J. Bloino, G. Zheng, J. L. Sonnenberg, M. Hada, M. Ehara, K. Toyota, R. Fukuda, J. Hasegawa, M. Ishida, T. Nakajima, Y. Honda, O. Kitao, H. Nakai, T. Vreven, J. A. Montgomery, Jr, J. E. Peralta, F. Ogliaro, M. Bearpark, J. J. Heyd, E. Brothers, K. N. Kudin, V. N. Staroverov, R. Kobayashi, J. Normand, K. Raghavachari, A. Rendell, J. C. Burant, S. S. Iyengar, J. Tomasi, M. Cossi, N. Rega, J. M. Millam, M. Klene, J. E. Knox, J. B. Cross, V. Bakken, C. Adamo, J. Jaramillo, R. Gomperts, R. E. Stratmann, O. Yazyev, A. J. Austin, R. Cammi, C. Pomelli, J. W. Ochterski, R. L. Martin, K. Morokuma, V. G. Zakrzewski, G. A. Voth, P. Salvador, J. J. Dannenberg, S. Dapprich, A. D. Daniels, Ö. Farkas, J. B. Foresman, J. V. Ortiz, J. Cioslowski, and D. J. Fox, *Gaussian 09, Revision A.02*, Gaussian, Inc., Wallingford CT, 2009.
22 http://www.pdb.org/.
23 S. Becker, B. Groner and C. W. Müller, *Nature*, 1998, **934**, 145–151.
24 A. Pedretti, L. Villa and G. Vistoli, *J. Mol. Graphics Modell.*, 2002, **21**, 47–49.
25 J. Gasteiger and M. Marsili, *Croat. Chem. Acta*, 1980, **53**, 601–614.
26 A. D. MacKerell Jr, D. Bashford, M. Bellott, R. L. Dunbrack Jr, J. D. Evanseck, M. J. Field, S. Fischer, J. Gao, H. Guo, S. Ha, D. Joseph-McCarthy, L. Kuchnir, K. Kuczera, F. T. K. Lau, C. Mattos, S. Michnick, T. Ngo, D. T. Nguyen, B. Prodhom, W. E. Reiher, III, B. Roux, M. S. chlenkrich, J. C. Smith, R. Stote, J. Straub, M. Watanabe, J. Wiorkiewicz-Kuczera, D. Yin and M. Karplus, *J. Phys. Chem. B*, 1998, **102**, 3586–3616.
27 N. Foloppe and A. D. MacKerell Jr, *J. Comput. Chem.*, 2000, **21**, 86–104.
28 J. C. Phillips, R. Braun, W. Wang, J. Gumbart, E. Tajkhorshid, E. Villa, C. Chipot, R. D. Skeel, L. Kale and K. Schulten, *J. Comput. Chem.*, 2005, **26**, 1781–1802.
29 D. S. Goodsell and A. J. Olson, *Proteins: Struct., Funct., Genet.*, 1990, **8**, 195–202.